Journal of Advanced Research 25 (2020) 147–157

Contents lists available at ScienceDirect

Journal of Advanced Research

journal homepage: www.elsevier.com/locate/jare

Multidimensional scaling locus of memristor and fractional order elements

J.A. Tenreiro Machado [a], António M. Lopes [b,*]

[a] Institute of Engineering, Polytechnic of Porto, Dept. of Electrical Engineering, Porto, Portugal
[b] UISPA–LAETA/INEGI, Faculty of Engineering, University of Porto, Porto, Portugal

HIGHLIGHTS

- Generalization of the periodic table of elements.
- Inclusion of fractional order elements.
- 2- and 3-dimensional maps of elements organized accordingly to their features.

GRAPHICAL ABSTRACT

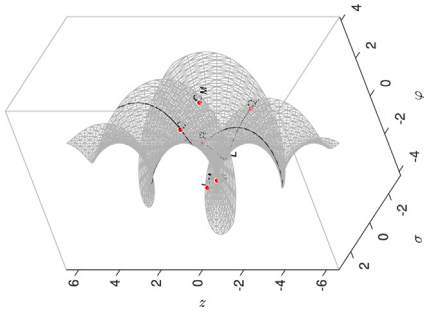

ARTICLE INFO

Article history:
Received 13 November 2019
Revised 3 January 2020
Accepted 8 January 2020
Available online 20 January 2020

Keywords:
Fractional calculus
Memristor
Information visualization
Multidimensional scaling
Procrustes analysis

ABSTRACT

This paper combines the synergies of three mathematical and computational generalizations. The concepts of fractional calculus, memristor and information visualization extend the classical ideas of integro-differential calculus, electrical elements and data representation, respectively. The study embeds these notions in a common framework, with the objective of organizing and describing the "continuum" of fractional order elements (FOE). Each FOE is characterized by its behavior, either in the time or in the frequency domains, and the differences between the FOE are captured by a variety of distinct indices, such as the Arccosine, Canberra, Jaccard and Sørensen distances. The dissimilarity information is processed by the multidimensional scaling (MDS) computational algorithm to unravel possible clusters and to allow a direct pattern visualization. The MDS yields 3-dimensional loci organized according to the FOE characteristics both for linear and nonlinear elements. The new representation generalizes the standard Cartesian 2-dimensional periodic table of elements.

Introduction

Leibniz (1646–1716) extended the differential calculus to the paradigm known as "Fractional Calculus" (FC) [1,2]. However, the FC remained an abstract tool restricted to the area of mathematics. The first application of FC is usually credited to Abel (1802–1829) with the so-called tautochrone curve problem [3,4]. Later we find the work of Heaviside (1850–1925), who fist applied such ideas in the scope of the operational calculus and electromagnetism [5,6]. Nonetheless, it was during the last two decades that FC was recognized as a good tool to characterize complex phenomena, due to the ability of describing adequately non-locality and long-range memory effects [7–11].

Paynter (1923–2002) formulated one systematic approach to modeling and invented the so-called bond graphs [12]. He consid-

Peer review under responsibility of Cairo University.
* Corresponding author.
E-mail addresses: jtm@isep.ipp.pt (J.A. Tenreiro Machado), aml@fe.up.pt (A.M. Lopes).

https://doi.org/10.1016/j.jare.2020.01.004
2090-1232/

ered 4 generalized variables, namely the effort, flow, momentum and displacement {*e*,*f*,*p*,*q*} so that $p = \int e(t)\mathrm{d}t$ and $q = \int f(t)\mathrm{d}t$. In page 136 of his class notes [12] he designed a diagram including the 4 state variables with vertex of a "tetrahedron of state". Paynter characterized the functional relationship between the 4 variables that are associated with the edges of the tetrahedron. The relations for $e-f$, $e-q$ and $p-f$ (for resistance, capacitance and inductance, respectively) were marked by continuous lines. Identically for $p-e$ and $q-f$ (for the integral/differential relationships). However, the relation $p-q$ was merely marked with a dashed line and no particular importance was given to it.

In 1971 Chua [13] noticed again the symmetries in the electrical integer order elements (IOE) and variables. Chua speculated that 4 elements were necessary to preserve a Cartesian arrangement. By other words, in his opinion, besides the standard 3 elements represented by the resistor, capacitor and inductor, a 4-th one, the so-called "memristor" or resistor with memory, was also necessary. In 2008 these ideas were brought to light in the scope of a laboratory experiment [14] and the topic became popular in a variety of applications.

The Chua [15] periodic table of elements (PTE) organizes two-terminal IOE in a 2-dimensional Cartesian matrix. Besides including IOE the generalization to real- and complex-order elements was also proposed [16,17]. However, the necessity of the 4-th element and the Cartesian layout of the PTE is still under debate [18,19]. In fact, this type of organization may not be the best one to accommodate the elements. It is out of the scope of the present paper to address the problem of writing systems, that is the method of visually representing communication. We recall that the Greek alphabet and consequent systems, settled on a left-to-right pattern, from the top to the bottom of the page. Nonetheless, Arabic and Hebrew scripts are written right-to-left, while those including Chinese characters were traditionally written vertically top-to-bottom and from the right to the left of the page. Therefore, we can question up to what point are we "prisoners" of our cultural heritage (https://en.wikipedia.org/wiki/Writing_system#Directionality). Furthermore, present day computational techniques for data processing and information visualization can provide superior forms of representation.

Information visualization involves the computer construction of some type of graphical representations, that otherwise would require more efforts to be interpreted, and helps to unravel patterns embedded in the data [20,21]. Due to the multidimensional nature of most data, the information visualization can take advantage of dimensionality reduction [22] and clustering [23] techniques.

This paper adopts information visualization to organize two-terminal fractional order elements (FOE). The new representation generalizes the 2-dimensional PTE by means of 3-dimensional loci of FOE. We verify that the FOE form a "continuum" where the IOE are special cases, and not the opposite, as often assumed. Therefore, without lack of generality, in the follow-up we shall mention as FOE to all elements. The proposed numerical and computational approach includes 2 phases. First, we characterize the FOE either in the time or in the frequency domains. The comparison of the FOE characteristics is performed by means of four metrics, namely the Arccosine, Canberra, Jaccard and Sørensen distances. Second, we process the dissimilarities through the multidimensional scaling (MDS) visualization computational method, that produces loci representative of the input information. The computational portraits are not restricted neither to 2-dimensional nor to Cartesian concepts based on human notions. Indeed, the FOE loci reveal distinct patterns that are built upon the distance metrics properties.

Following these thoughts, the paper has the following organization. Section 2 presents the concepts supporting the mathematical and computational methods. Section 3 characterizes the FOE by distinct methods, namely in the time and frequency domains. Additionally the FOE are compared with four distances and the information is processed by means of the MDS technique. Section 4 compares the effect of nonlinearities by means of Procrustes analysis. Finally, Section 5 draws the most important conclusions.

Mathematical and computational concepts

Fractional calculus

FC generalizes the concept of differentiation and integration to non integer and complex orders [24,25]. We find a variety of applications of FC, such as in control, physics, anomalous diffusion, and many others [26–29]. Fractional derivatives and integrals are non-local operators that capture the history dynamics, contrary to what happens with integer derivatives. Fractional systems have a memory of the dynamical evolution and many natural and artificial phenomena revealed these characteristics [7–10,30–32].

The most used definitions of fractional derivative are the Riemann-Liouville, Grünwald-Letnikov and Caputo formulations [33–35]. For certain functions, the fractional derivative follows closely their integer order version. For example, at steady state, a sinusoidal function with amplitude A and phase Φ has the derivative of order $\alpha \in \mathbb{R}$ given by [36]:

$$\frac{\mathrm{d}^\alpha}{\mathrm{d}t^\alpha}[A\cos(\omega t+\Phi)] = A\omega^\alpha \cos\left(\omega t+\Phi+\alpha\frac{\pi}{2}\right), \tag{1}$$

where $\frac{\mathrm{d}^\alpha}{\mathrm{d}t^\alpha}$ denotes the fractional derivative or order α, t represents time, and f and $\omega = 2\pi f$ are the frequency and angular frequency, respectively.

In the frequency domain, for zero initial conditions and the function $x(t)$, we can write:

$$\mathcal{L}\left\{\frac{\mathrm{d}^\alpha}{\mathrm{d}t^\alpha}x(t)\right\} = s^\alpha \mathcal{L}\{x(t)\}, \tag{2}$$

$$\mathcal{F}\left\{\frac{\mathrm{d}^\alpha}{\mathrm{d}t^\alpha}x(t)\right\} = (j\omega)^\alpha \mathcal{F}\{x(t)\}, \tag{3}$$

where $\mathcal{L}\{\cdot\}$ and $\mathcal{F}\{\cdot\}$ represent the Fourier and Laplace operators, s stands for the Laplace variable and $j = \sqrt{-1}$.

The frequency dependent negative conductance and negative resistance

The frequency dependent negative conductance and frequency dependent negative resistance (FDNC and FDNR) were introduced in 1969 and 1971 by Bruton [37] and Antoniou [38]. The electronic implementation of these elements have been under progress during the last decades [39-42]. The FDNC and FDNR are denoted by *D*- and *N*-elements and are usually considered with linear behavior, having admittance and impedance $\mathbf{Y}(s) = \mathbf{Z}^{-1}(s) = Ds^2$ and $\mathbf{Z}(s) = Ns^2$, respectively. These devices are often adopted in ladder filters without inductors [37] and chaotic oscillators [43].

The FDNC and FDNR require an implementation using active devices and, although not passive, demonstrate that they are feasible and useful. Moreover, for circuit branch impedances $\mathbf{Z}_i(s) = k_i s^{n_i}, k_i \in \mathbb{R},\ n_i \in \mathbb{N},\ i = 1,2,\cdots$, of integer order we obtain also an integer order input impedance $\mathbf{Z}(s)$. On the other hand, if we use fractional impedances $\mathbf{Z}_i(s) = k_i s^{\alpha_i}, \alpha_i \in \mathbb{R}$, then we can obtain $\mathbf{Z}(s)$ both integer and fractional [44].

The memristor

The magnetic flux and the electrical charge, $\phi(t)$ and $q(t)$, are related to the voltage and current, $v(t)$ and $i(t)$, by:

$$\phi(t) = \int_{-\infty}^{t} v(\tau)d\tau, \quad q(t) = \int_{-\infty}^{t} i(\tau)d\tau. \tag{4}$$

In linear circuits, the resistor, inductor and capacitor, R, L and C, follow the relations:

$$v(t) = Ri(t), \quad \phi(t) = Li(t), \quad q(t) = Cv(t). \tag{5}$$

The "memristor" M is the element verifying the relation [45–50]:

$$\phi(t) = M(q)q(t). \tag{6}$$

If we have a linear relationship between ϕ and q, then $M(q) = M$ similarly to a resistance, since $\frac{d\phi}{dt} = M\frac{dq}{dt} \Longleftrightarrow v = Mi$.

The generalization of the memristor concept to a larger class, the so-called "memristive systems", is also possible [15,51–53]. The charge-controlled memristor and flux-controlled memconductance are modeled by the expressions:

$$\phi = \widehat{\phi}(q), q = \widehat{q}(\phi), \tag{7}$$

and their time derivatives yield:

$$v = \frac{\partial\widehat{\phi}(q)}{\partial q} i, \quad i = \frac{\partial\widehat{q}(\phi)}{\partial\phi} v, \tag{8}$$

where $M_i(q) = \frac{\partial\widehat{\phi}(q)}{\partial q}$ and $M_v(\phi) = \frac{\partial\widehat{q}(\phi)}{\partial\phi}$ are the incremental memristor and memconductance, respectively.

The expressions (8) establish that $i = 0 \Rightarrow v = 0$ and $v = 0 \Rightarrow i = 0$, independently of q and ϕ, respectively. Again, if the models (7) are linear, then we obtain the resistance R and conductance G, respectively.

If we consider the generalized relations:

$$\sigma(t) = \int_{-\infty}^{t} q(\tau)d\tau, \quad \rho(t) = \int_{-\infty}^{t} \phi(\tau)d\tau, \tag{9}$$

then we have [54]:

$$\sigma = \widehat{\sigma}(\phi), \quad \rho = \widehat{\rho}(q), \tag{10}$$

$$q = C_M(\phi)v, \quad \phi = L_M(q)i, \tag{11}$$

where $C_M(\phi) = \frac{\partial\widehat{\sigma}(\phi)}{\partial\phi}$ and $L_M(q) = \frac{\partial\widehat{\rho}(q)}{\partial q}$ stand for the incremental memcapacitor and meminductor, respectively. Similarly to what occurs with $M_i(q)$ and $M_v(\phi)$, the elements $C_M(\phi)$ and $L_M(q)$ "remember" the flux and charge previously applied. These ideas support the so-called one-port higher order element, establishing a relation between $v(t)$ and $i(t)$, such that:

$$\frac{d^m}{dt^m} v(t) = \psi\left(\frac{d^n}{dt^n} i(t)\right), m, n \in \mathbb{Z}. \tag{12}$$

Linearizing expression (12) around some operating point $Q = \left(\frac{d^m}{dt^m} v_Q, \frac{d^n}{dt^n} i_Q\right)$ on the element characteristic (12), we obtain:

$$\frac{d^n}{dt^n}(v - v_Q) = m_Q \cdot \frac{d^m}{dt^m}(i - i_Q), \tag{13}$$

where m_Q denotes the slope of the line tangent to the characteristic $\frac{d^m}{dt^m} v(t) = \psi\left(\frac{d^n}{dt^n} i(t)\right)$ at point Q.

In the frequency domain, expression (13) yields:

$$\mathbf{V}(j\omega) = \mathbf{Z}(j\omega)\mathbf{I}(j\omega), \tag{14}$$

where

$$\mathbf{Z}(j\omega) = (j\omega)^{n-m} \cdot m_Q, \tag{15}$$

is the small-signal impedance of the element at the operating point Q.

Based on those concepts, the PTE was proposed [15] as represented in Fig. 1. Each point (m, n) represents an IOE and we verify that: (i) there are four element categories that repeat *ad infinitum* along the $\Gamma-$diagonal lines; (ii) if we take any (m, n) IOE and add (subtract) a multiple of four to either m or n, or to both m and n, then we obtain a higher (lower) order IOE of the same category;

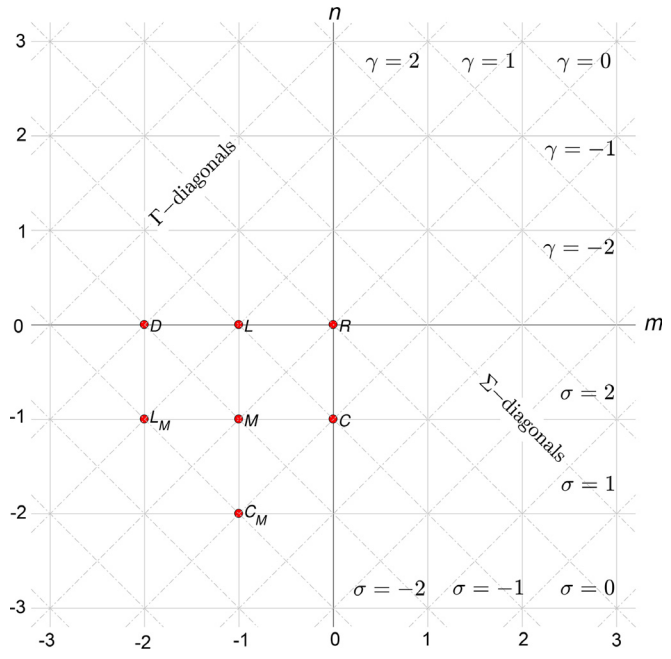

Fig. 1. Simplified Cartesian representation of the PTE of two-terminal IOE. The acronyms stand for resistor, inductor, frequency dependent negative conductance, capacitor, memristor, meminductor, memcapacitor.

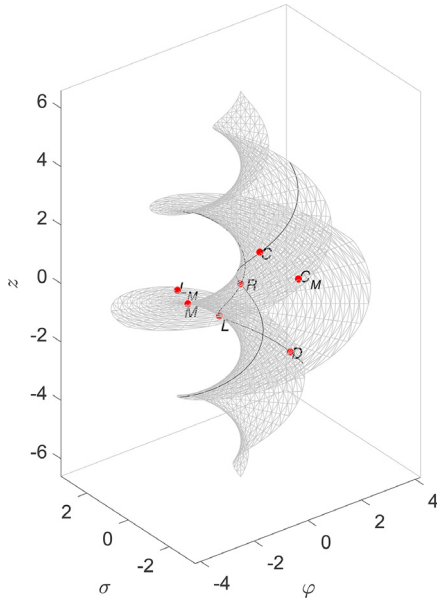

Fig. 2. The 3-dimensional representation of the PTE of two-terminal IOE using the coordinate transformation (16). The acronyms $\{R, L, D, C, M, L_M, C_M\}$ stand for {resistor, inductor, frequency dependent negative conductance, capacitor, memristor, meminductor, memcapacitor}.

(iii) if we add or subtract 1 to both m and n, then we move the (m,n) IOE along its $\Gamma-$diagonal line to the new position $(m+1,n+1)$, maintaining the IOE category; (iv) both the local and the global properties of all IOE on any $\Gamma-$diagonal line are preserved; (v) the cases $(m,n)=\{(0,0),(-1,0),(-2,0),(0,-1),(-1,-1),(-2,-1),(-1,-2)\}$ stand for $\{R,L,D,C,M,L_M,C_M\}$. The location of the elements in the PTE may also be specified by other types of coordinates. For example, if we choose the coordinates (σ,γ), where $\sigma=n+m$ and $\gamma=n-m$, then all IOE with the same value σ/γ lie on one of the $\Sigma/\Gamma-$diagonals and the element of coordinates (σ,γ) is at the intersection of both lines. Moreover, the $\Sigma-$diagonals are occupied either by resistive or reactive IOE, for even or odd values of σ, respectively [55].

The classical PTE represents only IOE and, therefore, we are restricted to $\gamma\in\mathbb{Z}$. However, other non-planar and non-Cartesian arrangements are possible for representing the IOE. If we apply the coordinate transformation $(m,n)\rightarrow(\varphi,\sigma,z)$, such that

$$\varphi=(m-n)\cdot\frac{\pi}{2},\quad \sigma=m+n, z=\varphi, \tag{16}$$

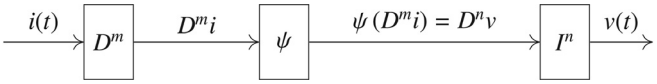

Fig. 3. Block diagram of a FOE where $\psi(\cdot)$ is some linear/nonlinear function: input $i(t)$ and output $v(t)$ given by $x_{d,e}(t)=A_e\cos(\omega_d t)$ and $z_{d,e}(t)=\psi\left[A_e\omega_d^{\gamma_n}\cos(\omega_d t+\gamma_n\frac{\pi}{2})\right]$, respectively.

then we obtain the 3-dimensional PTE illustrated in Fig. 2. With this representation, R is located at the center of the spiral-like locus and the elements in the diagonals are represented at horizontal lines.

In another point of view, a closer look to the standard PTE reveals that the space in the middle of the grid lines is, in fact, the locus for the FOE. Indeed, it is known the existence of fractional inductors and capacitors [56–60] and, therefore, the generalization of the PTE to a "continuum" of FOE is the logical step to follow [61].

Distance functions

We adopt a set of 4 distances, $\{\delta_A,\delta_C,\delta_J,\delta_S\}$, to measure the dissimilarity between pairs $(\mathbf{P}_n,\mathbf{P}_p)$ of objects with real and imaginary components [62]. Therefore, the items are characterized by $K\times 2$ dimensional matrices $\mathbf{P}_n=\left[[\mathrm{Re}\{P_{n1}\}\cdots,\mathrm{Re}\{P_{nK}\}]^T,[\mathrm{Im}\{P_{n1}\},\cdots,\mathrm{Im}\{P_{nK}\}]^T\right]$ and $\mathbf{P}_p=\left[[\mathrm{Re}\{P_{p1}\},\cdots,\mathrm{Re}\{P_{pK}\}]^T,[\mathrm{Im}\{P_{p1}\},\cdots,\mathrm{Im}\{P_{pK}\}]^T\right]$, where $\mathrm{Re}\{\cdot\}$ and $\mathrm{Im}\{\cdot\}$ stand for the real and imaginary parts. The distances are given by the expressions:

$$\delta_A(\mathbf{P}_n,\mathbf{P}_p)=\arccos\left(\frac{\sum_{k=1}^{K}\mathrm{Re}\{P_{nk}\}\mathrm{Re}\{P_{pk}\}+\sum_{k=1}^{K}\mathrm{Im}\{P_{nk}\}\mathrm{Im}\{P_{pk}\}}{\sqrt{\sum_{k=1}^{K}Re\{P_{nk}\}^2+Im\{P_{nk}\}^2}\sqrt{\sum_{k=1}^{K}Re\{P_{pk}\}^2+Im\{P_{pk}\}^2}}\right), \tag{17}$$

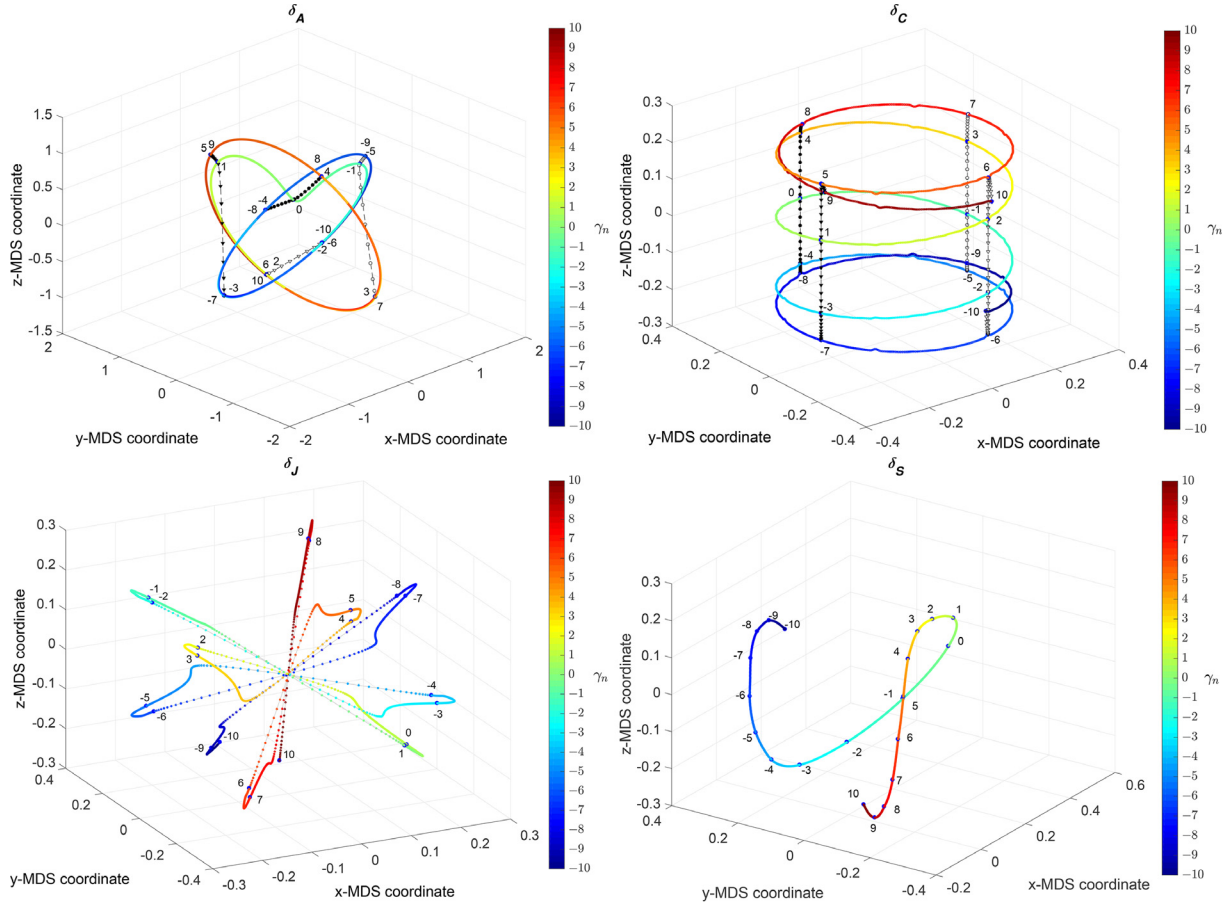

Fig. 4. The 3-dimensional loci of $N=721$ linear FOE, characterized in the time domain by means of the distances: (a) δ_A; (b) δ_C; (c) δ_J; (d) δ_S. The markers represent the FOE and their color varies with the FOE order $\gamma_n\in[-10,10]$. The other parameters are $N_\omega=40$, $\omega_d\in\left[10^{-1},10^{1}\right]$, $N_A=1$, $N_t=1000$ and $N_p=5$. In the loci (a) and (b) the IOE of the same category are connected with dashed lines.

$$\delta_C(\mathbf{P}_n,\mathbf{P}_p)=\sum_{k=1}^{K}\frac{|\mathrm{Re}\{P_{nk}\}-\mathrm{Re}\{P_{pk}\}|}{|\mathrm{Re}\{P_{nk}\}|+|\mathrm{Re}\{P_{pk}\}|}+\sum_{k=1}^{K}\frac{|\mathrm{Im}\{P_{nk}\}-\mathrm{Im}\{P_{pk}\}|}{|\mathrm{Im}\{P_{nk}\}|+|\mathrm{Im}\{P_{pk}\}|}, \tag{18}$$

$$\delta_J(\mathbf{P}_n,\mathbf{P}_p)=\frac{\sum_{k=1}^{K}\left(Re\{P_{nk}\}-Re\{P_{pk}\}\right)^2}{\sum_{k=1}^{K}Re\{P_{nk}\}^2+\sum_{k=1}^{K}Re\{P_{pk}\}^2-\sum_{k=1}^{K}Re\{P_{nk}\}Re\{P_{pk}\}}+\frac{\sum_{k=1}^{K}\left(Im\{P_{nk}\}-Im\{P_{pk}\}\right)^2}{\sum_{k=1}^{K}Im\{P_{nk}\}^2+\sum_{k=1}^{K}Im\{P_{pk}\}^2-\sum_{k=1}^{K}Im\{P_{nk}\}Im\{P_{pk}\}}. \tag{19}$$

$$\delta_S(\mathbf{P}_n,\mathbf{P}_p)=\frac{\sum_{k=1}^{K}|Re\{P_{nk}\}-Re\{P_{pk}\}|+\sum_{k=1}^{K}|Im\{P_{nk}\}-Im\{P_{pk}\}|}{\sum_{k=1}^{K}|Re\{P_{nk}\}+Re\{P_{pk}\}|+\sum_{k=1}^{K}|Im\{P_{nk}\}+Im\{P_{pk}\}|}. \tag{20}$$

If the objects to be compared have no imaginary part, then the vectors $\mathbf{P}_n$ and $\mathbf{P}_p$ are $K\times 1$ dimensional, and the set $\{\delta_A,\delta_C,\delta_J,\delta_S\}$ corresponds to the standard {Arccosine, Canberra, Jaccard, Sørensen} distances [63].

We must note that other distances are possible [63] and that several of them were also tested. By other words, we are not restricted to the standard Cartesian concepts, neither for in the chart nor for the difference measurements. It is well known that the Cartesian perspective is a particular case of the Minkowski formulation and that this is just a family of distances within a plethora of generalized expressions [62,63]. However, further distances are not included herein for sake of parsimony, since $\{\delta_A,\delta_C,\delta_J,\delta_S\}$ illustrate adequately the proposed concepts.

Multidimensional scaling

The MDS is a computational recursive method that provides dimensionality reduction and envisages to produce a locus with clusters and, possibly, some data organization capable of being visualized and interpreted [64–66]. Given a set of N objects K-dimensional and a dissimilarity index, we calculate a $N\times N$ matrix, $\Delta=[\delta_{np}]$, $n,p=1,\cdots,N$, of object-to-object dissimilarities, such that $\delta_{np}=\delta_{pn}$ and $\delta_{nn}=0$. This information represents the input of the visualization algorithm. The MDS represents the N objects by points in a W-dimensional space, with $W<K$, and tries to reproduce the measured dissimilarities. The MDS iterates the estimate of point configuration for optimizing a given fitness, achieving a matrix of distances $\widehat{\Delta}=\left[\widehat{\delta}_{np}\right]$, $n,p=1,\cdots,N$, that approximates the original one $\Delta=[\delta_{np}]$. A common fitness is the raw stress:

$$\mathcal{S}=\sum_{n=2}^{N}\sum_{p=1}^{n-1}\left[\hat{\delta}_{np}-\theta(\delta_{np})\right]^2, \tag{21}$$

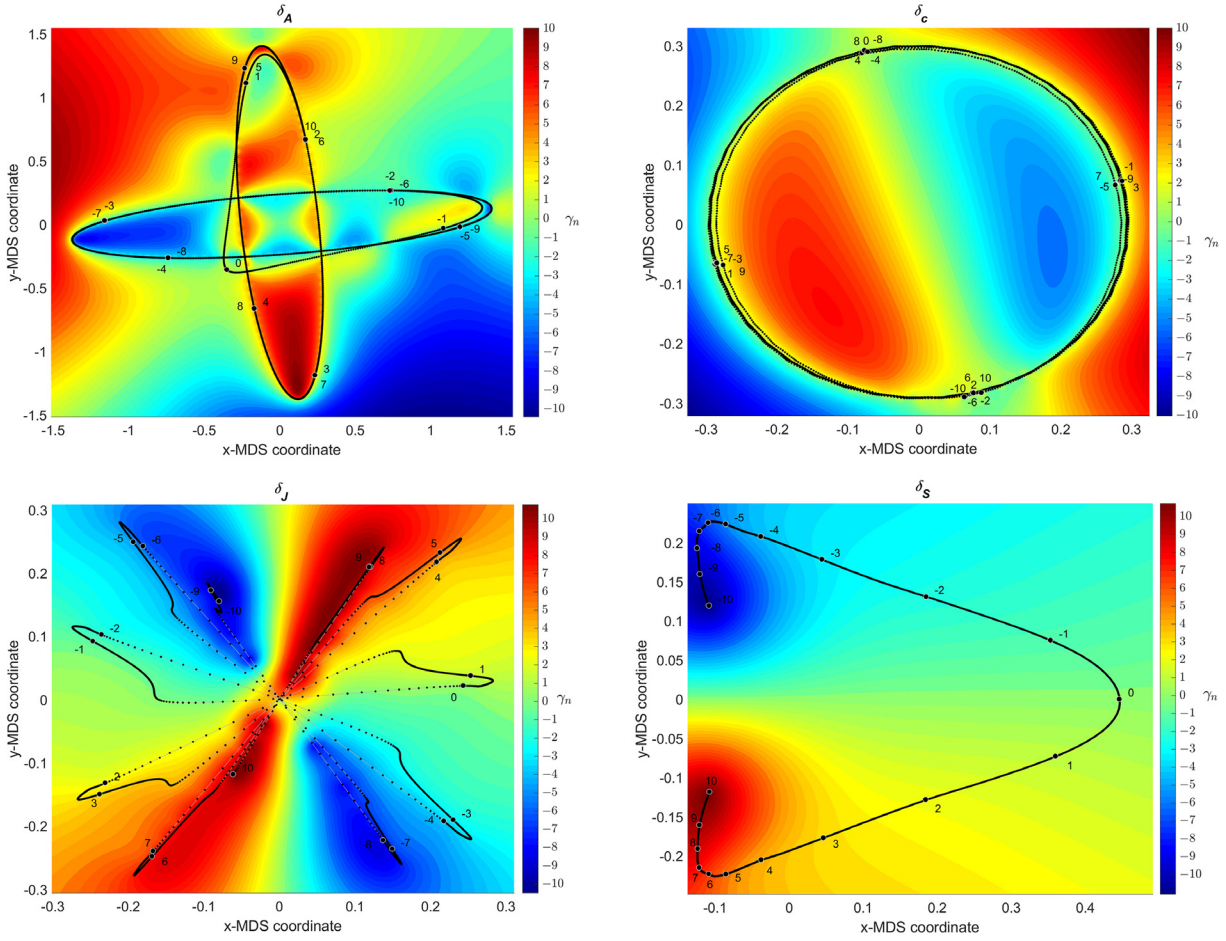

Fig. 5. The 2 + 1-dimensional loci of $N=721$ linear FOE, characterized in the time domain by means of the distances: (a) δ_A; (b) δ_C; (c) δ_J; (d) δ_S. The z coordinate of the loci is calculated by means of RBI based on the value of $\gamma_n\in[-10,10]$ at each MDS (x,y) coordinate. The other parameters are $N_\omega=40$, $\omega_d\in\left[10^{-1},10^{1}\right]$, $N_A=1$, $N_t=1000$ and $N_p=5$

where $\theta(\cdot)$ denotes some kind of linear or nonlinear transformation.

The MDS interpretation is based on the clusters and patterns in the W-dimensional locus and not in the individual coordinates of the points. Points that are close (distant) in the W-dimensional locus represent similar (dissimilar) objects in the K-dimensional space. We can translate, rotate and magnify the locus to provide a better visualization. The MDS axes have no units and no special physical meaning.

The MDS quality can be verified through the Shepard and stress plots. The first compares the resulting and the original distances, $\widehat{\delta}_{np}$ and δ_{np}, for a given value of W. Therefore, a narrow (large) dispersion of the points represents a good (poor) fit between $\widehat{\delta}_{np}$ and δ_{np}. On the other hand, the stress plot represents $\mathcal{S}$ versus W and is a monotonically decreasing function. Usually the values $W = 2$ or $W = 3$ are adopted, because they allow a straightforward computational visualization and establish a compromise between low values of $\mathcal{S}$ or W.

Visualizing fractional order elements

In this Section we generate several MDS representations both of linear and nonlinear FOE. Firstly, we describe the FOE by their behavior either in the time or in the frequency domains. This information will represent the objects **P**, that is, the FOE. Secondly, we use the resulting data for comparing the FOE and calculate the dissimilarity matrix Δ measured by means of a given distance function δ. Finally, we feed the data into the MDS for constructing the matrix $\widehat{\Delta}$ and the W-dimensional loci of FOE.

Let us consider the set of N FOE of orders $\Gamma = \{\gamma_n : \gamma_{min} \leq \gamma_n \leq \gamma_{max}, n = 1, \cdots, N\}$. To each FOE we apply a collection of sinusoidal signals $x_{d,e}(t) = A_e \cos(\omega_d t)$ with frequencies $\Omega = \{\omega_d : \omega_{min} \leq \omega_d \leq \omega_{max}, d = 1, \cdots, N_\omega\}$. For nonlinear systems the set of testing amplitudes is given by $\mathbf{A} = \{A_e : A_{min} \leq A_e \leq A_{max}, e = 1, \cdots, N_A\}$, but, obviously, for the linear case we can use just one value ($N_A = 1$). Then we compute the $N_\omega \cdot N_A$ system outputs $z_{d,e}(t) = \psi\left[A_e \omega_d^{\gamma_n} \cos\left(\omega_d t + \gamma_n \frac{\pi}{2}\right)\right]$, where ψ represents some kind of linear/nonlinear function, $t = l \cdot t_d$, $l = 0, 1, \cdots, N_t - 1$ and $t_d = N_p \cdot \frac{2\pi}{\omega_d (N_t - 1)}$, with t_d denoting the sampling period, N_t standing for the number of time samples, and N_p representing the number of periods of the signals (Fig. 3).

During the experiments some effect of truncating the series of γ_n values, that is, of limiting to γ_{min} and γ_{max} was observed on the produced loci. Therefore, to reduce that effect, all experiments adopted some extra values at both extremes that are not represented.

Time domain analysis and visualization of linear fractional order elements

In this case we compare linear FOE in the time domain, meaning that we consider $N_A = 1$. Therefore, after collecting the N_ω outputs

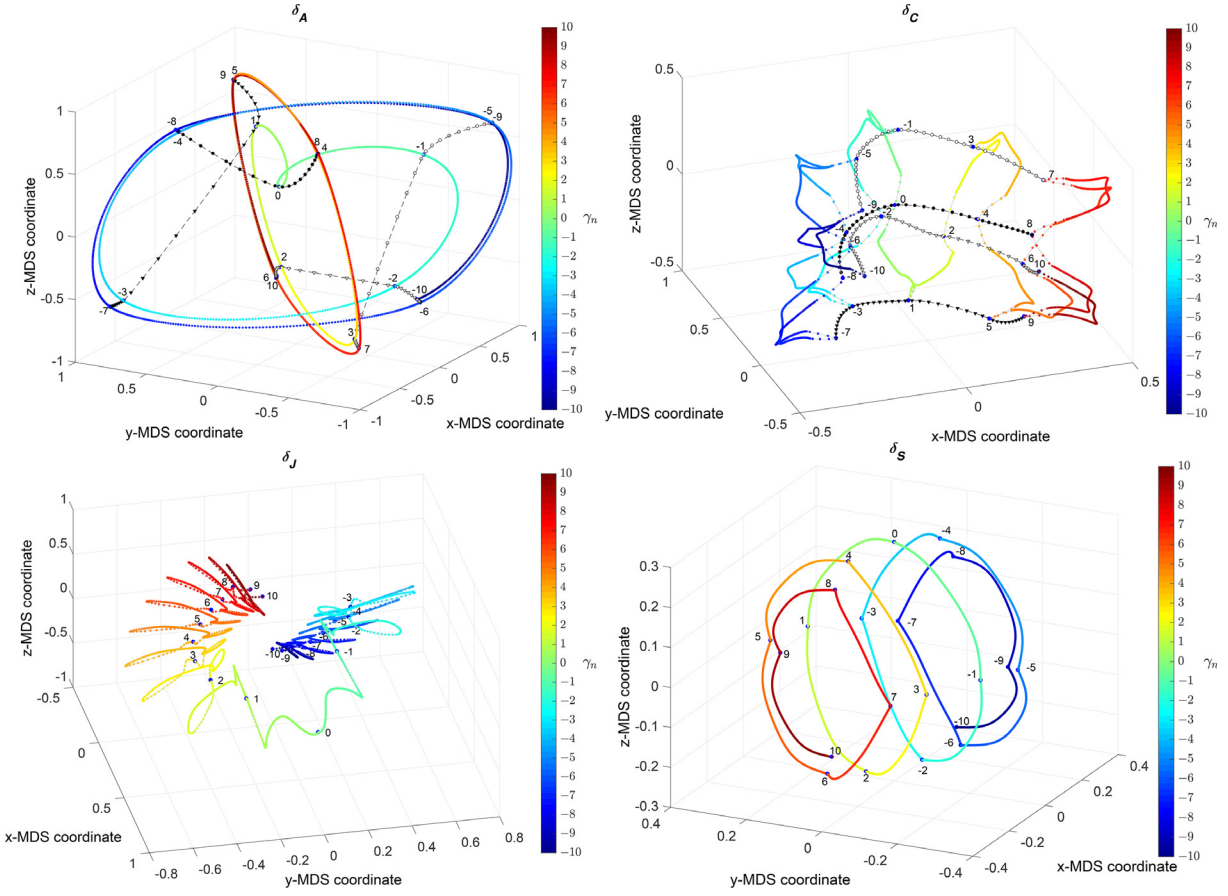

Fig. 6. The 3-dimensional loci of $N = 721$ linear FOE, characterized in the frequency domain by means of the distances: (a) δ_A; (b) δ_C; (c) δ_J; (d) δ_S. The markers represent the FOE and their color varies with the FOE order $\gamma_n \in [-10, 10]$. The other parameters are $N_\omega = 40$, $\omega_d \in \left[10^{-1}, 10^{1}\right]$, $N_A = 1$, $N_t = 1000$ and $N_p = 5$. In the loci (a) and (b) the IOE of the same category are connected with dashed lines.

of the n-th FOE, we construct the $K = N_t \cdot N_\omega$ dimensional real-valued vectors $\mathbf{P}_n(t) = [z_{1,1}(t), \cdots, z_{N_\omega,1}(t)]$ and calculate the distance matrices $\Delta = [\delta(\mathbf{P}_n(t), \mathbf{P}_p(t))]$, $n, p = 1, \cdots, N$, where $\delta(\mathbf{P}_n(t), \mathbf{P}_p(t))$ denotes one distance of the set $\{\delta_A, \delta_C, \delta_J, \delta_S\}$ between the vectors $\mathbf{P}_n(t)$ and $\mathbf{P}_p(t)$ given by expressions (17)–(20). Finally, we process each matrix Δ by means of the MDS for constructing the FOE loci.

Fig. 4 depicts the 3-dimensional MDS loci of $N = 721$ linear FOE with order values spaced linearly in the interval $-10 \leq \gamma_n \leq 10$, when adopting $N_\omega = 40$ test frequencies spaced logarithmically in the interval $10^{-1} \leq \omega_d \leq 10^{1}$, $N_t = 1000$ time samples and $N_p = 5$ periods. Several distinct amplitudes were tested numerically, but, as expected, the FOE loci do not depend on this parameter. All other parameters were adjusted by successively increasing their values until the loci are insensitive to changes. The markers represent the FOE and the colors vary with the FOE order, γ_n, to enhance the visualization. In the loci (a) and (b) the IOE of the same category are connected by dashed lines. Such lines are not included in (c) and (d), since for their good visualization we need to rotate the charts. For all distances, we verify that the FOE form smooth patterns, exhibiting regularities that depend on the FOE categories. Moreover, the representations do not follow the standard Cartesian arrangement and use efficiently the 3-dimensional visualization space.

Variations to the previous loci are possible to highlight specific aspects of the organization of the FOE and to capture distinct information provided by the MDS computational scheme. These possibilities are illustrated in Fig. 5, where we consider two MDS dimensions for the (x, y) coordinates, while the z coordinate is calculated by means of radial basis interpolation (RBI) [67] of the FOE order γ_n. The thin-plate spline RBI function, $\phi(\varepsilon) = \varepsilon^2 \log\varepsilon$, is considered, where the variable ε denotes the Euclidean distance between the points generated by the 2-dimensional MDS. Nonetheless, we believe that the 3-dimensional visualization of the locus is more advantageous than the 2+1-dimensional portrait. Therefore, for reducing length, in the follow-up we restrict to the richer visualization method.

Frequency domain analysis and visualization of linear fractional order elements

For the n-th FOE, $n = 1, \cdots, N$, we convert the sinusoidal outputs $z_{d,1}(t)$, $d = 1, \cdots, N_\omega$, to the Fourier domain, yielding $\mathcal{F}\{z_{d,1}(t)\} = \mathbf{Z}_{d,1}(j\omega)$, where $\omega = \omega_d$. We generate the $N_\omega \times 2$ dimensional complex-valued matrix $\mathbf{P}_n(\omega) = [\mathrm{Re}\{\mathbf{Z}_{d,1}(j\omega)\}, \mathrm{Im}\{\mathbf{Z}_{d,1}(j\omega)\}]$ and calculate the dissimilarity matrices Δ that feed the MDS algorithm and generate the FOE loci.

Fig. 6 depicts the 3-dimensional loci of the $N = 721$ linear FOE, characterized in the frequency domain by means of the distances $\{\delta_A, \delta_C, \delta_J, \delta_S\}$. The values of the parameters are identical to those adopted in the Subsection 3.1. For all distances we verify that the linear FOE loci do not depend on the amplitude of the sinusoidal inputs

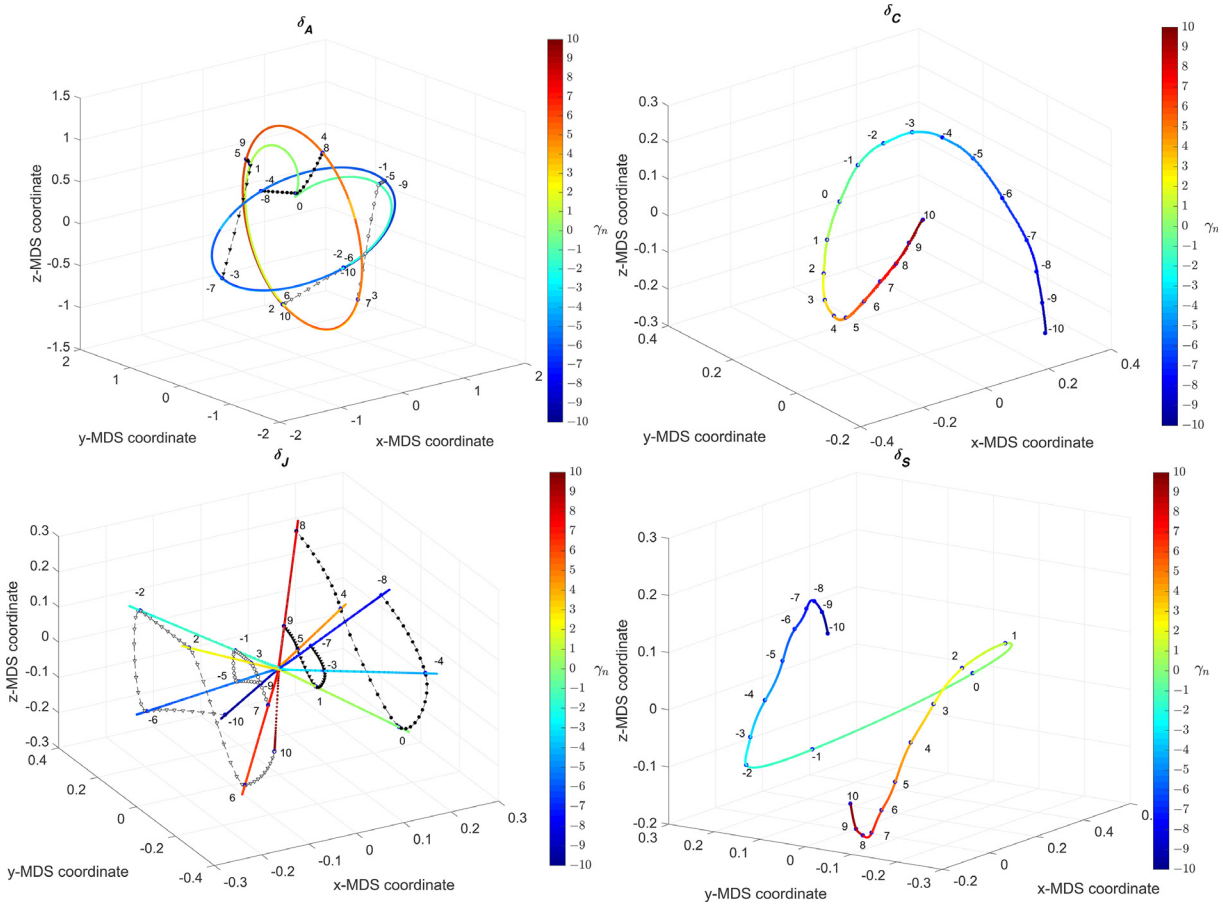

Fig. 7. The 3-dimensional loci of $N = 721$ nonlinear (ψ of degree 3) FOE, characterized in the time domain by means of the distances: (a) δ_A; (b) δ_C; (c) δ_J; (d) δ_S. The markers represent the FOE and their color varies with the FOE order $\gamma_n \in [-10, 10]$. The other parameters are $N_\omega = 40$, $\omega_d \in \left[10^{-1}, 10^{1}\right]$, $N_A = 10$, $N_e \in \left[10^{-2}, 10^{2}\right]$, $N_t = 1000$ and $N_p = 5$. In the loci (a) and (c) the IOE of the same category are connected with dashed lines.

and that the loci form smooth patterns with regularities that depend on the FOE categories. The charts are different from those obtained in the time domain, but follow an identical logic, namely using a non-Cartesian arrangement in a 3-dimensional space.

Time domain analysis and visualization of nonlinear fractional order elements

In this case we compare nonlinear FOE in the time domain adopting for ψ a cubic nonlinearity. We must note that other nonlinearities [68] are possible and that several were tested. However, they are not included herein for sake of parsimony, since this one illustrates well the proposed ideas.

For the n-th nonlinear FOE, $n = 1, \cdots, N$, we collect $N_\omega \cdot N_A$ outputs, $z_{d,e}(t)$, where $d = 1, \cdots, N_\omega$ and $e = 1, \cdots, N_A$. Then, for comparing the FOE, we construct the $K = N_t \cdot N_\omega \cdot N_A$ dimensional real-valued vectors $\mathbf{P}_n(t) = [z_{1,1}(t), \ldots, z_{1,N_A}(t), \ldots, z_{N_\omega,1}(t), \ldots, z_{N_\omega,N_A}(t)]$. Finally, we calculate the distance matrices $\Delta = [\delta(\mathbf{P}_n, \mathbf{P}_p)]$, $n, p = 1, \cdots, N$, and apply the MDS numerical algorithm. Fig. 7 depicts the 3-dimensional MDS loci of the $N = 721$ nonlinear FOE, characterized in the time domain by means of $\{\delta_A, \delta_C, \delta_J, \delta_S\}$. The values of the parameters are identical to those adopted in the previous Subsections, but for the nonlinear case we consider $N_A = 10$ amplitudes of the input signal spaced logarithmically in the interval $10^{-2} \le N_e \le 10^2$. Comparing Figs. 7 and 4, we verify that the loci generated with the distances $\{\delta_A, \delta_S\}$ do not vary, while those generated with $\{\delta_C, \delta_J\}$ vary considerably with the presence of the nonlinearity. We verify again that we can adjust the characteristics of the loci, in this case the sensitivity to the nonlinearity ψ, by a judicious choice of the proper distance.

Frequency domain analysis and visualization of nonlinear fractional order elements

We compare $N = 721$ nonlinear FOE in the frequency domain adopting for ψ the cubic nonlinearity.

In a first phase, for the n-th FOE, $n = 1, \cdots, N$, we convert the $N_\omega \cdot N_A$ outputs $z_{d,e}(t)$ to the Fourier domain, yielding $\mathcal{F}\{z_{d,e}(t)\} = \mathbf{Z}_{d,e}(j\omega)$, noting that for a cubic nonlinearity $z_{d,e}(t)$ has the first and third harmonics. In a second phase, for comparing the FOE, we generate the $(2 \cdot N_\omega \cdot N_A) \times 2$ dimensional complex-valued array $\mathbf{P}_n(\omega) = [\mathrm{Re}\{\mathbf{Z}_{d,e}(j\omega)\}, \mathrm{Im}\{\mathbf{Z}_{d,e}(j\omega)\}]$. Finally, we calculate the dissimilarity matrices Δ, and generate the MDS FOE loci.

Fig. 8 depicts the 3-dimensional MDS loci of the $N = 721$ nonlinear FOE, characterized in the frequency domain. All values of the parameters are kept unchanged from the previous Subsections.

Procrustes analysis and visualization of nonlinear fractional order elements

In this Section, we compare the loci obtained with different nonlinearities by means of Procrustes analysis [69–72]. The Pro-

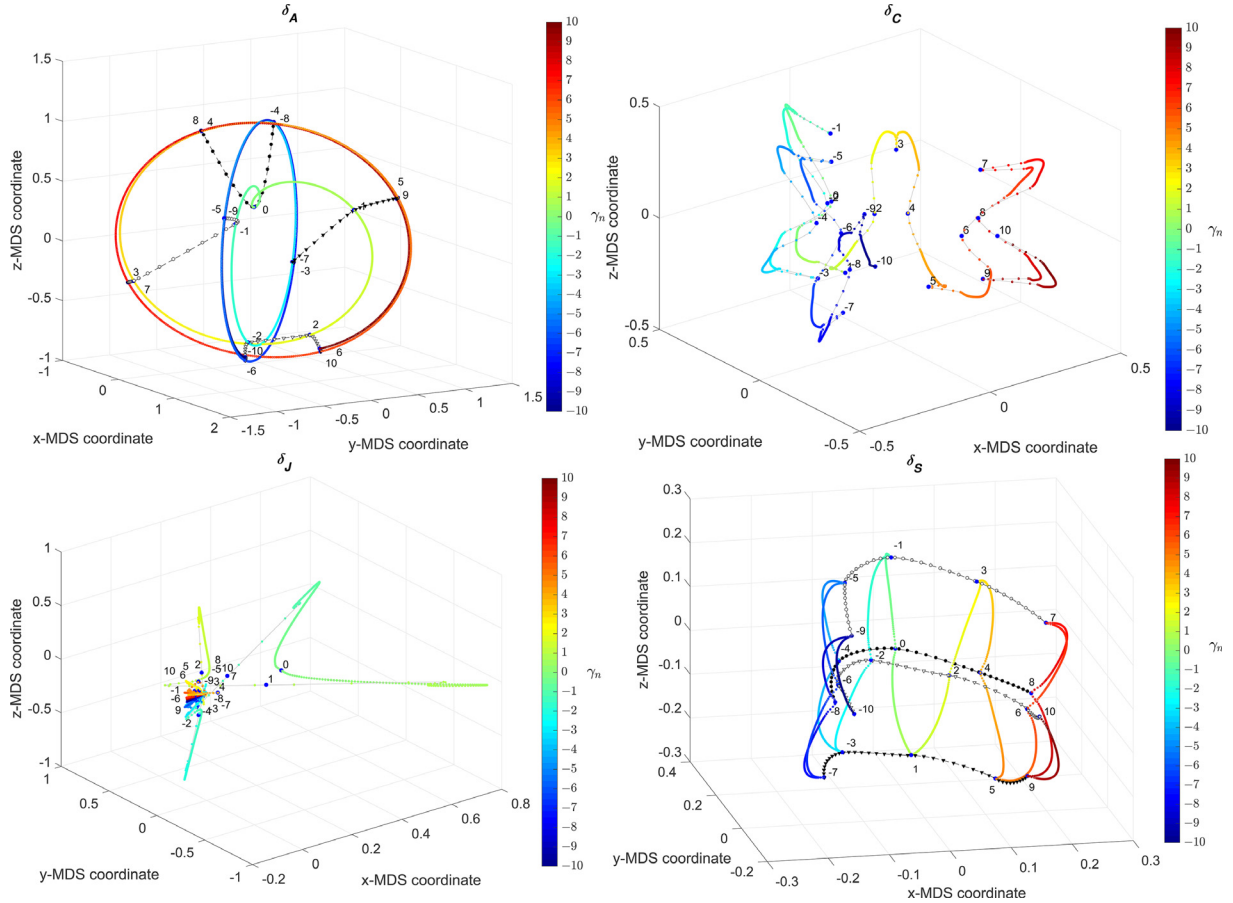

Fig. 8. The 3-dimensional loci of $N = 721$ nonlinear (ψ of degree 3) FOE, characterized in the frequency domain by means of the distances: (a) δ_A; (b) δ_C; (c) δ_J; (d) δ_S. The markers represent the FOE and their color varies with the FOE order $\gamma \in [-10, 10]$. The other parameters are $N_\omega = 40$, $\omega_d \in \left[10^{-1}, 10^{1}\right]$, $N_A = 10$, $N_e \in \left[10^{-2}, 10^{2}\right]$, $N_t = 1000$ and $N_p = 5$. In the loci (a) and (d) the IOE of the same category are connected with dashed lines.

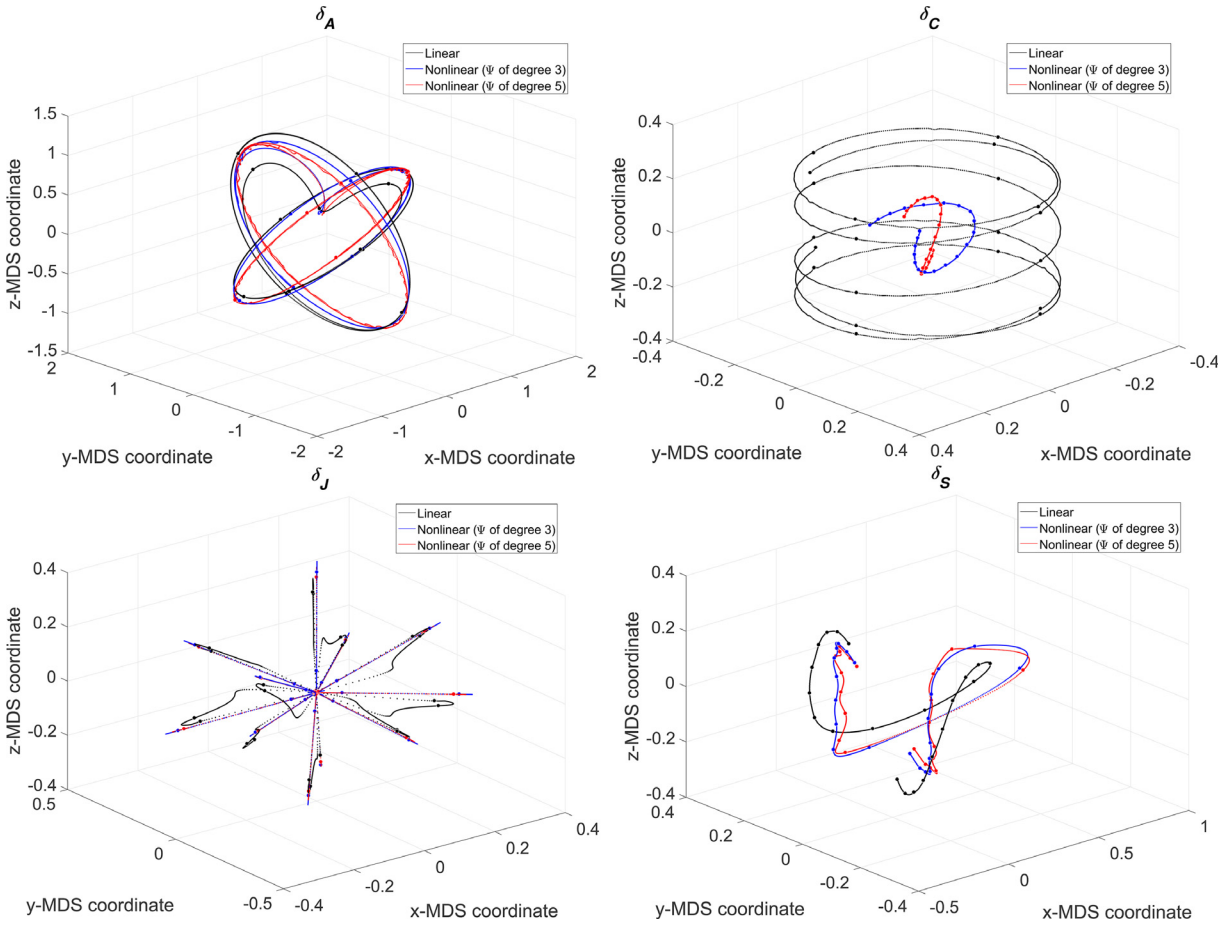

Fig. 9. Three superimposed 3-dimensional loci of $N = 721$ FOE (using Procrustes), characterized in the time domain by means of the distances: (a) δ_A; (b) δ_C; (c) δ_J; (d) δ_S. The functions ψ of degree 1 (linear case), 3 and 5 are adopted.

crustes analysis takes a collection of loci and transforms them for obtaining the "best" superposition. The algorithm performs four iterative numerical steps: (i) the user chooses a reference locus (by selecting one of the available instances); (ii) superimposes all other loci into the current reference by means of linear transformations, namely translation, reflection, orthogonal rotation and scaling; (iii) computes the mean form of the current set of superimposed loci; (iv) compares the distance between the mean and the reference instances to a given threshold value and, if above, sets the reference to the mean form and continues to step (ii). The result is a global representation of all loci that best conforms them.

Figs. 9 and 10 depict three superimposed 3-dimensional MDS loci of $N = 721$ FOE (using Procrustes), characterized in the time and frequency domains, respectively. Besides the linear case we adopt power law nonlinearities ψ of degree 3 and 5. The values of all parameters are identical to those used in the previous Section. We verify an evolution of the loci with n, demonstrating the sensitivity of the technique to the nonlinearity. For the distances δ_A and δ_S this evolution is smooth, while for δ_C and δ_J we obtain a sharp transition between the linear and the nonlinear cases, when the FOE are characterized in the time and the frequency domains, respectively. Therefore, we verify that we can extend the construction of the MDS loci and their comparison to other types of nonlinearites.

Conclusions

This paper used clustering and information visualization techniques to organize and map FOE accordingly to their characteristics. The new representation generalizes the concept of PTE, revealing that the integer order cases are just a limited number of cases in the FOE "continuum". The use of the MDS allows exploring the 3-dimensional space for the representation and the adoption of distinct measures, so that users can choose the one fitting better their needs. The technique is effective both in the time and frequency domains and can be extended from linear to nonlinear elements. Moreover, the study provides a complementary perspective in the on-going discussion about the properties of the memristor and fractional-order elements. Indeed, a new form of representation, based in distinct domains and distances, may shed further light into possible similarities or dissimilarities between elements.

In summary, this paper did not intend to give responses to a variety of possible questions such as if there are finite boundaries, or not, to the Chua's PTE, or what is the physical meaning of fractional elements. The study shows that we are often conditioned by representations methods that can be bettered by modern computer-based information visualization algorithms. Furthermore, in the scope of the new visualization methods, the use of Cartesian concepts, namely for graphical representations and for

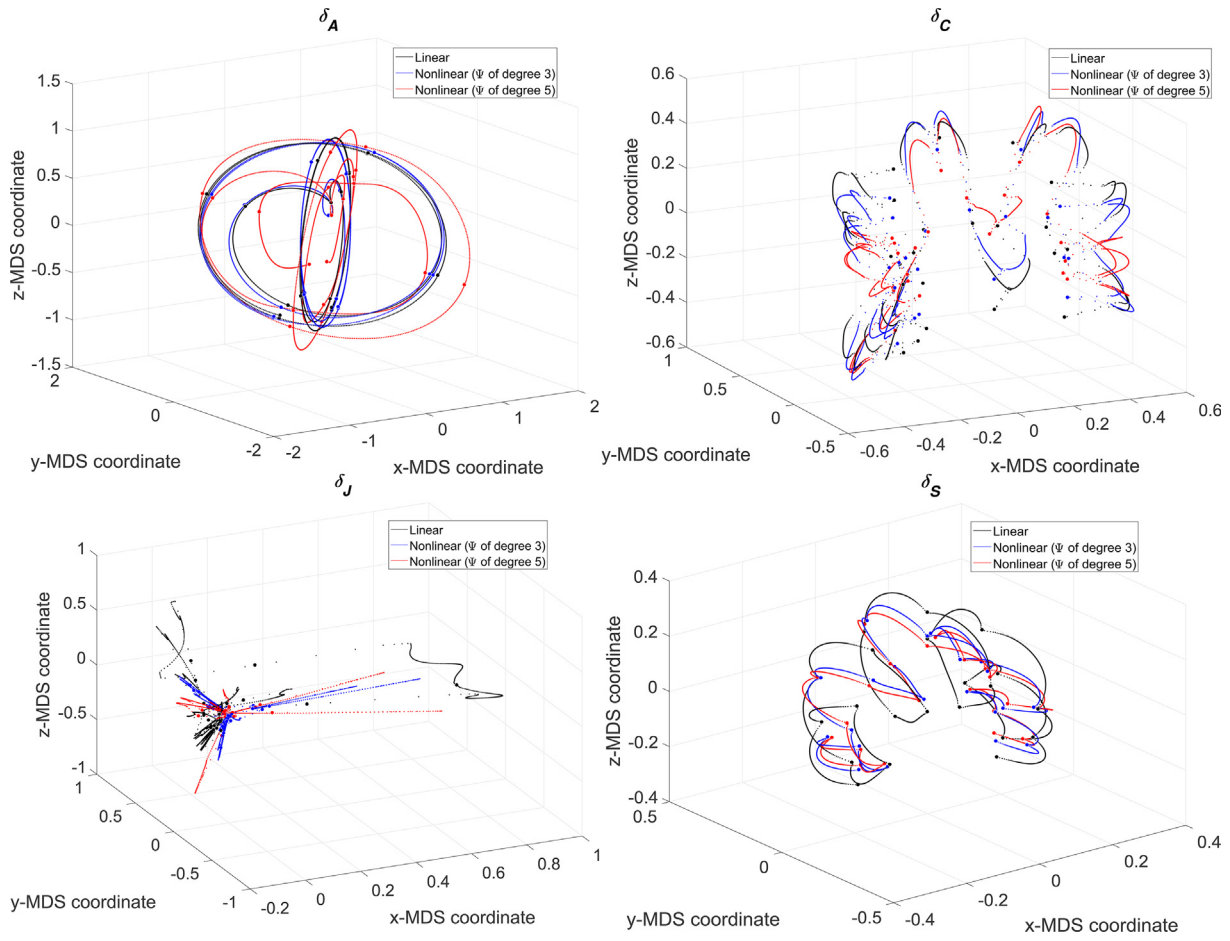

Fig. 10. Three superimposed 3-dimensional loci of $N = 721$ FOE (using Procrustes), characterized in the frequency domain by means of the distances: (a) δ_A; (b) δ_C; (c) δ_J; (d) δ_S. The functions ψ of degree 1 (linear case), 3 and 5 are adopted.

distance (or difference) assessment, can be outperformed by a careful selection of the formulation that fits better a specific application.

Declaration of Competing Interest

The authors declare that they have no known competing financial interests or personal relationships that could have appeared to influence the work reported in this paper.

Acknowledgement

Fundação para a Ciência e Tecnologia, Portugal, Reference: Projeto LAETA - UID/EMS/50022/2013.

References

[1] Ross B. Fractional calculus. Math Mag 1977;50(3):115–22.
[2] Yang X-J, Baleanu D, Srivastava HM. Local fractional integral transforms and their applications. London: Academic Press; 2015.
[3] Valério D, Machado JT, Kiryakova V. Some pioneers of the applications of fractional calculus. Fract Calculus Appl Anal 2014;17(2):552–78.
[4] Tenreiro Machado JA, Kiryakova Virginia, Kochubei Anatoly, Luchko Yuri. Recent history of the fractional calculus: data and statistics. In: Kochubei Anatoly, Luchko Yuri, editors. Basic theory. Berlin, Boston: De Gruyter; 2019. p. 1–22. doi: https://doi.org/10.1515/9783110571622-001.
[5] Josephs HJ. Oliver Heaviside papers found at Paignton in 1957. Inst Electric Eng 1959;319:70–6.
[6] Mahon B. Oliver Heaviside: maverick mastermind of electricity. London: Institution of Engineering and Technology; 2009.
[7] Machado JA Tenreiro, Lopes António M, Tarasov Vasily E. Fractional Van der Pol oscillator. In: Tarasov Vasily E, editor. Applications in physics, Part A. Berlin, Boston: De Gruyter; 2019. p. 1–22. doi: https://doi.org/10.1515/9783110571707-001.
[8] Valério D, Ortigueira M, Machado JT, Lopes AM. Continuous-time fractional linear systems: Steady-state behaviour. In: Petráš, I, editor, Handbook of fractional calculus with applications: applications in engineering, life and social sciences, Part A, vol. 6. Berlin: De Gruyter. p. 149–74.
[9] Lopes António M, Tenreiro Machado JA, Băleanu Dumitru, Mendes Lopes António. Fractional-order modeling of electro-impedance spectroscopy information. In: Băleanu Dumitru, Mendes Lopes António, editors. Applications in engineering, life and social sciences, part A. Berlin, Boston: De Gruyter; 2019. p. 21–42. doi: https://doi.org/10.1515/9783110571905-002.
[10] Parsa B, Dabiri A, Machado JAT. Application of variable order fractional calculus in solid mechanics. In: Baleanu D, Lopes AM, editors. Handbook of fractional calculus with applications: applications in engineering, life and social sciences, Part A, Vol. 7. Berlin: De Gruyter. p. 207–24.
[11] Machado JT, Lopes AM. Relative fractional dynamics of stock markets. Nonlinear Dyn 2016;86(3):1613–9.
[12] Paynter H. Analysis and design of engineering systems: Class notes for M.I.T. course 2.751. Boston: M.I.T. Press; 1961.
[13] Chua LO. Memristor - the missing circuit element. IEEE Trans Circuit Theory 1971;18(2):507–19.
[14] Dmitri DB, Strukov B, Snider GS, Stewart DR, Williams RS. The missing memristor found. Nature 2008;97:80–3.
[15] Di Ventra M, Pershin YV, Chua LO. Circuits elements with memory: memristors, memcapacitors and meminductors. Proc IEEE 2009;97(10):1717–24.
[16] Abdelouahab M-S, Lozi R, Chua L. Memfractance: A mathematical paradigm for circuit elements with memory. Int J Bifurcation Chaos 2014;24(09):1430023.
[17] Wang FZ, Shi L, Wu H, Helian N, Chua LO. Fractional memristor. Appl Phys Lett 2017;111(24):243502.
[18] Abraham I. The case for rejecting the memristor as a fundamental circuit element. Sci Rep 2018;8(1):10972.
[19] Wang FZ. A triangular periodic table of elementary circuit elements. IEEE Trans Circuits Syst I Regul Pap 2013;60(3):616–23.
[20] Ware C. Information visualization: perception for design. Waltham: Elsevier; 2012.

[21] Spence R. Information visualization: An introduction, Vol. 1. Cham: Springer; 2001.
[22] Van Der Maaten L, Postma E, Van den Herik J. Dimensionality reduction: a comparative review. J Mach Learn Res 2009;10:66–71.
[23] Jain AK, Murty MN, Flynn PJ. Data clustering: a review. ACM Comput Surv (CSUR) 1999;31(3):264–323.
[24] Podlubny I. Fractional differential equations, Volume 198: An Introduction to Fractional derivatives, fractional differential equations, to methods of their solution, mathematics in science and engineering. San Diego: Academic Press; 1998.
[25] Kilbas A, Srivastava H, Trujillo J. Theory and applications of fractional differential equations, Vol. 204, North-Holland mathematics studies. Amsterdam: Elsevier; 2006.
[26] Oustaloup A. Systèmes asservis linéaires d'ordre fractionnaire: Théorie et pratique. Paris: Masson; 1983.
[27] Machado JAT. Analysis and design of fractional-order digital control systems. Syst Anal, Model, Simul 1997;27(2–3):107–22.
[28] Tarasov VE. Fractional dynamics: Applications of fractional calculus to dynamics of particles, fields and media. Beijing, Heidelberg: Springer; 2010.
[29] Mainardi F. Fractional calculus and waves in linear viscoelasticity: an introduction to mathematical models. London: Imperial College Press; 2010.
[30] Gómez-Aguilar J, Yépez-Martnez H, Escobar-Jiménez R, Astorga-Zaragoza C, Reyes-Reyes J. Analytical and numerical solutions of electrical circuits described by fractional derivatives. Appl Math Model 2016;40(21–22):9079–94.
[31] Gómez-Aguilar JF, Dumitru B. Fractional transmission line with losses. Zeitschrift für Naturforschung A 2014;69(10–11):539–46.
[32] Ionescu C, Lopes A, Copot D, Machado JT, Bates J. The role of fractional calculus in modeling biological phenomena: a review. Commun Nonlinear Sci Numer Simul 2017;51:141–59.
[33] Ortigueira MD, Machado JT, Coito FJV, Bengochea G. Discrete-time fractional signals and systems. In: Baleanu D, Lopes AM, editors. Handbook of fractional calculus with applications: applications in engineering, life and social sciences, part B, Vol. 8. Berlin: De Gruyter. p. 207–24.
[34] Ortigueira MD, Machado JT. What is a fractional derivative? J Comput Phys 2015;293:4–13.
[35] Teodoro GS, Machado JT, De Oliveira EC. A review of definitions of fractional derivatives and other operators. J Comput Phys 2019;388:195–208.
[36] Valério D, Trujillo JJ, Rivero M, Machado JT, Baleanu D. Fractional calculus: a survey of useful formulas. Eur Phys J Spec Topics 2013;222(8):1827–46.
[37] Bruton L. Network transfer functions using the concept of frequency-dependent negative resistance. IEEE Trans Circuit Theory 1969;16(3):406–8. doi: https://doi.org/10.1109/TCT.1969.1082989.
[38] Antoniou A. Novel RC-active-network synthesis using generalized immittance converters. IEEE Trans Circuit Theory 1970;17(2):212–7.
[39] Soliman AM, Saad RA. Two new families of floating FDNR circuits. J Electric Comput Eng 2010;2010:7. Article ID 563761.
[40] Psychalinos C, Pal K, Vlassis S. A floating generalized impedance converter with current feedback operational amplifiers. AEU-Int J Electron Commun 2008;62(2):81–5.
[41] Senani R, Bhaskar D. Versatile voltage-controlled impedance configuration. IEE Proc-Circ, Dev Syst 1994;141(5):414–6.
[42] Pal K. Novel FDNC simulation using current conveyors. Electron Lett 1980;16 (16):639–41.
[43] Elwakil AS, Kennedy MP. Chaotic oscillator configuration using a frequency dependent negative resistor. Int J Circuit Theory Appl 2000;28(1):69–76.
[44] Kapoulea S, Tsirimokou G, Psychalinos C, Elwakil AS. Generalized fully adjustable structure for emulating fractional-order capacitors and inductors of orders less than two. Circ, Syst, Signal Process 2019:1–18.
[45] Mladenov V. Advanced memristor modeling: memristor circuits and networks. MDPI; 2019.
[46] Hajtó D, Rák Á, Cserey G. Robust memristor networks for neuromorphic computation applications. Materials 2019;12(21):3573.
[47] Nguyen TV, Pham KV, Min K-S. Hybrid circuit of memristor and complementary metal-oxide-semiconductor for defect-tolerant spatial pooling with boost-factor adjustment. Materials 2019;12(13):2122.
[48] Ordonez-Miranda J, Ezzahri Y, Tiburcio-Moreno JA, Joulain K, Drevillon J. Radiative thermal memristor. Phys Rev Lett 2019;123(2):025901.
[49] Semary MS, Fouda ME, Hassan HN, Radwan AG. Realization of fractional-order capacitor based on passive symmetric network. J Adv Res 2019;18:147–59.
[50] Wu J, Wang G, Iu HH-C, Shen Y, Zhou W. A nonvolatile fractional order memristor model and its complex dynamics. Entropy 2019;21(10):955.
[51] Chua LO, Kang SM. Memristive devices and systems. Proc IEEE 1976;64 (2):209–23.
[52] Chua LO, Kang SM. Device modeling via basic nonlinear circuits elements. IEEE Trans Circ Syst 1980;27(11):1014–44.
[53] Chua LO. Nonlinear circuit foundations for nanodevices, Part I: The four-element torus. Proc IEEE 2003;91(11):1830–59.
[54] Jeltsema D, Dòria-Cerezo A. Port-Hamiltonian formulation of systems with memory. Proc IEEE 2012;100(6):1928–37.
[55] Biolek Z, Biolek D, Biolkova V. Lagrangian for circuits with higher-order elements. Entropy 2019;21(11):1059.
[56] Westerlund S. Dead matter has memory. Kalmar, Sweden: Causal Consulting; 2002.
[57] Bohannan GW. Analog realization of a fractional control element – revisited. In: Proc. of the 41st IEEE Int. Conf. on Decision and Control, Tutorial Workshop 2: Fractional Calculus Applications in Automatic Control and Robotics, Las Vegas, USA; 2002.
[58] Biswas K, Sen S, Dutta PK. Realization of a constant phase element and its performance study in a differentiator circuit. IEEE Trans Circuits Syst II Express Briefs 2006;53(9):802–6.
[59] Tenreiro Machado JA, Galhano AM. Fractional order inductive phenomena based on the skin effect. Nonlinear Dyn 2012;68(1–2):107–15.
[60] Radwan AG, Soliman A, Elwakil AS, Sedeek A. On the stability of linear systems with fractional-order elements. Chaos, Solitons Fractals 2009;40(5):2317–28.
[61] Machado JT. Fractional generalization of memristor and higher order elements. Commun Nonlinear Sci Numer Simul 2013;18(2):264–75.
[62] Cha S-H. Comprehensive survey on distance/similarity measures between probability density functions. Int J Math Models Methods Appl Sci 2007;1 (4):300–7.
[63] Deza MM, Deza E. Encyclopedia of distances. Berlin Heidelberg: Springer-Verlag; 2009.
[64] Saeed Nasir, Nam Haewoon, Haq Mian Imtiaz Ul, Muhammad Saqib Dost Bhatti. A survey on multidimensional scaling. ACM Comput. Surv 2018;51 (3):1–25. doi: https://doi.org/10.1145/321270910.1145/3178155.
[65] Machado JT, Lopes AM. Multidimensional scaling analysis of soccer dynamics. Appl Math Model 2017;45:642–52.
[66] Machado JT, Lopes AM. A fractional perspective on the trajectory control of redundant and hyper-redundant robot manipulators. Appl Math Model 2017;46:716–26.
[67] Carr JC, Fright WR, Beatson RK. Surface interpolation with radial basis functions for medical imaging. IEEE Trans Med Imaging 1997;16(1):96–107.
[68] Machado J. Visualizing non-linear control system performance by means of multidimensional scaling. J Comput Nonlinear Dyn 2013;8(4):041017.
[69] Bookstein FL. Landmark methods for forms without landmarks: Morphometrics of group differences in outline shape. Med Image Anal 1997;1(3):225–43.
[70] Gower JC, Dijksterhuis GB. Procrustes problems, Vol. 3. Oxford: Oxford University Press; 2004.
[71] Lopes AM, Tenreiro Machado J, Galhano AM. Multidimensional scaling visualization using parametric entropy. Int J Bifurcat Chaos 2015;25 (14):1540017.
[72] Tenreiro Machado J, Lopes AM, Galhano AM. Multidimensional scaling visualization using parametric similarity indices. Entropy 2015;17 (4):1775–94.